Semi-automatic delimitation of volcanic edifice boundaries: Validation and application to the cinder cones of the Tancitaro–Nueva

Geomorphology 219 (2014) 152–160

Contents lists available at ScienceDirect

Geomorphology

journal homepage: www.elsevier.com/locate/geomorph

Semi-automatic delimitation of volcanic edifice boundaries: Validation and application to the cinder cones of the Tancitaro–Nueva Italia region (Michoacán–Guanajuato Volcanic Field, Mexico)

Federico Di Traglia [a,b,1], Stefano Morelli [a,*], Nicola Casagli [a,2], Victor Hugo Garduño Monroy [c,3]

[a] Department of Earth Sciences, University of Firenze, Via La Pira n°4, 50121 Firenze, Italy
[b] Department of Earth Sciences, Università di Pisa, Via Santa Maria n°53, 56126 Pisa, Italy
[c] Instituto de Investigaciones en Ciencias de la Tierra, Universidad Michoacana de San Nicolás de Hidalgo, Ciudad Universitaria, Edif. U, 58030 Morelia, Michoacán, Mexico

ARTICLE INFO

Article history:
Received 21 January 2014
Received in revised form 5 May 2014
Accepted 11 May 2014
Available online 15 May 2014

Keywords:
Cinder cones
Volcano landform
Digital Elevation Model
Vent distribution
Morphometry
Michoacán–Guanajuato Volcanic Field

ABSTRACT

The shape and size of monogenetic volcanoes are the result of complex evolutions involving the interaction of eruptive activity, structural setting and degradational processes. Morphological studies of cinder cones aim to evaluate volcanic hazard on the Earth and to decipher the origins of various structures on extraterrestrial planets. Efforts have been dedicated so far to the characterization of the cinder cone morphology in a systematic and comparable manner. However, manual delimitation is time-consuming and influenced by the user subjectivity but, on the other hand, automatic boundary delimitation of volcanic terrains can be affected by irregular topography. In this work, the semi-automatic delimitation of volcanic edifice boundaries proposed by Grosse et al. (2009) for stratovolcanoes was tested for the first time over monogenetic cinder cones. The method, based on the integration of the DEM-derived slope and curvature maps, is applied here to the Tancitaro–Nueva Italia region of the Michoacán–Guanajuato Volcanic Field (Mexico), where 309 Plio-Quaternary cinder cones are located. The semi-automatic extraction allowed identification of 137 of the 309 cinder cones of the Tancitaro–Nueva Italia region, recognized by means of the manual extraction. This value corresponds to the 44.3% of the total number of cinder cones. Analysis on vent alignments allowed us to identify NE–SW vent alignments and cone elongations, consistent with a NE–SW σ_{max} and a NW–SE σ_{min}. Constructing a vent intensity map, based on computing the number of vents within a radius r centred on each vent of the data set and choosing $r = 5$ km, four vent intensity maxima were derived: one is positioned in the NW with respect to the Volcano Tancitaro, one in the NE, one to the S and another vent cluster located at the SE boundary of the studied area. The spacing of centroid of each cluster (24 km) can be related to the thickness of the crust (9–10 km) overlying the magma reservoir.

1. Introduction and rationale for the study

Monogenetic pyroclastic cones are the most common continental volcanic landforms on Earth. They commonly form extensive (over hundreds of km^2, and few to hundreds of cones) cinder-cone fields, sometimes associated with polygenetic shield volcanoes (Tibaldi, 1995; Dóniz et al., 2008; Kereszturi and Németh, 2012; Le Corvec et al., 2013a). Morphologic studies of cinder cones have undergone considerable improvement in recent decades (Martin and Németh, 2006; Németh et al., 2011; Kereszturi et al., 2012; Cimarelli et al., 2013; Kereszturi et al., 2013) and they have mainly aimed to evaluate volcanic hazard on the Earth (Connor et al., 2000; Le Corvec et al., 2013b) and to decipher the origins of various conical structures distinguished on spacecraft images of the extraterrestrial planets (Wood, 1980a; Broz and Hauber, 2012; Spudis et al., 2013).

The shape and size of monogenetic volcanoes are the result of complex geological evolutions involving the interaction of eruptive activity (different phases), tectonic/structural setting (vent distribution and alignment) and degradational (erosion) processes. The style of the monogenetic basaltic volcanism may range from Strombolian to Hawaiian to violent Strombolian, including phases of phreatomagmatism, depending on the behaviour of the exsolving volatile species, magma rise-speed, the coupling between gas and magma, and the interaction between magma and external water (Head and Wilson, 1989; Parfitt, 2004; Taddeucci et al., 2004; Valentine et al., 2005; Pioli et al., 2008; Valentine and Gregg, 2008; Andronico et al., 2009; Di Traglia et al., 2009; Cimarelli et al., 2010). Each monogenetic vent represents the

* Corresponding author. Tel.: +39 055 27557782; fax: +39 055 2757788.
E-mail addresses: federico.ditraglia@unifi.it (F. Di Traglia), stefano.morelli@unifi.it (S. Morelli), nicola.casagli@unifi.it (N. Casagli), vgmonroy@umich.mx (V.H. Garduño Monroy).
[1] Tel.: +39 055 2757782; fax: +39 055 2757788.
[2] Tel.: +39 055 2757523; fax: +39 055 2756296.
[3] Tel.: +52 443 3223500x4019; fax: +52 443 3223500x4010.

http://dx.doi.org/10.1016/j.geomorph.2014.05.002

surface expression of a single magma pathway from the crustal or mantle source (Takada, 1994; Valentine and Perry, 2007; Brenna et al., 2011; Le Corvec et al., 2013a). The propagation of magma-filled crack (dike) patterns is controlled by the actual regional tectonic stress field or by the pre-existing structure (Takada, 1994; Rubin, 1995; Gaffney and Damjanac, 2006; Valentine and Krogh, 2006; Gaffney et al., 2007; Le Corvec et al., 2013c). The geometry of the magma plumbing system, whether controlled by regional stress and/or pre-existing structures, is expressed at the Earth's surface by alignments of volcanic centres and by irregularities with respect to a perfectly conical morphology of the cinder cones (Connor, 1990; Tibaldi, 1995; Le Corvec et al, 2013a).

Several studies have been dedicated to the analysis of cinder cone morphology, with the aim of elucidating the cone growth/erosion rate (Wood, 1980a,b; Hasenaka and Carmichael, 1985; Favalli et al., 2009; Fornaciai et al., 2010; Bemis et al., 2011; Inbar et al., 2011; Kervyn et al., 2012; Rodriguez-Gonzalez et al., 2012; Kereszturi et al., 2013), the orientation of the regional and local stress field (Corazzato and Tibaldi, 2006; Mazzarini et al., 2010; Cebriá et al., 2011a; Pérez-López et al., 2011; Fornaciai et al., 2012; Cimarelli et al., 2013; Le Corvec et al., 2013b) and the relationship between the external cinder cone morphology and the internal deposit architecture, related to the different stage and eruptive style experienced by the cones (Martin and Németh, 2006; Cimarelli et al., 2013).

However, limited effort has been dedicated so far to the characterization of the cinder cone morphology in a systematic and comparable manner (Bohnenstiehl et al., 2012; Howell et al., 2012; Euillades et al., 2013). To measure morphometric features of individual cinder cones, complete closed-boundary delimitation is necessary. Currently most cinder cone delimitation is performed manually by visual identification and digitization on maps, Digital Elevation Models (DEMs), aerial photos or satellite images (Lesti et al., 2008; Beggan and Hamilton, 2010; Cimarelli et al., 2013; Le Corvec et al., 2013b). Manual delimitation is time-consuming and suffers from user subjectivity. On the other hand, automatic boundary delimitation of cinder cones with the available algorithms can be affected by irregular topography, when cinder cone fields developed on very rough landscapes such as those on stratovolcanoes (e.g. Mt Etna, Italy; Corazzato and Tibaldi, 2006) or on mountain belts (e.g. Garrotxa Volcanic Field, NE Spain; Cimarelli et al., 2013).

The aim of this study is to test on monogenetic volcanic fields the semiautomatic volcanic edifice boundary delimitation method proposed by Grosse et al. (2009, 2012), using a low-resolution (50 × 50 m pixel resolution) DEM. We chose a low-resolution topography because of the large global coverage of some satellite-derived low-resolution DEMs (SRTM, ASTER GDEM). Up to the present this method, based on the integration of DEM-derived information (such as the slope and the curvature), has been successfully applied only to the extraction of morphometric parameters of stratovolcanoes (Grosse et al., 2009, 2012; Di Traglia et al., 2013). So, the Tancitaro–Nueva Italia region (Fig. 1; Ownby et al., 2011), in the Michoacán–Guanajuato Volcanic Field (Mexico), thanks to the concentration of 309 Plio-Quaternary cinder cones, recognized by means of manual extraction (Hasenaka and Carmichael, 1985; Mazzarini et al., 2010; Cebriá et al., 2011a), has been chosen as the study area in which to explore the efficacy of this method.

2. Geological setting

The Michoacán–Guanajuato Volcanic Field (MGVF; Fig. 1) extends for about 40,000 km^2 along the central portion of the Trans-Mexican Volcanic Belt (TMVB) and contains over 1000 late Quaternary volcanic centres, of which approximately 90% are basaltic monogenetic cinder cones (Hasenaka and Carmichael, 1985; Connor, 1987, 1990). On the whole the entire volcanic arc is constituted by more than 8000 volcanic constructs and extends from the Gulf of California to the Gulf of Mexico (Connor, 1990). The TMVB is related to the subduction of the Rivera and Cocos tectonic plates underneath the North America Plate. The middle geometrical axis of the TMVB does not trend with a direction parallel to the Middle American Trench (MAT), but trends with a NW–SE direction from the west Pacific margin to the central part of the TMVB (Morelia city, Fig. 1), turning to E–W from Morelia to Veracruz city, and showing a deviation of 15ºW from the MAT (Fig. 1; Pérez-López et al., 2011 and references therein). Geologic evidence indicates that the TMVB is presently under an extensional tectonic regime, with a small and variable left-lateral component (Pasquare et al., 1990, 1991; Gómez-Tuena et al., 2007), which may be explained by considering the small degree of obliquity of the convergence between Cocos and North America plates (Mazzarini et al., 2010 and references therein). The TMVB is divided into three areas: (1) Western area; (2) Central area, where the MGVF is located; and (3) the Eastern Zone. Connor (1990) has divided the TMVB in eight clusters by using a search radius of 16 km for the whole set of 1016 cones. The MGVF lies in the Central area, while other volcanic fields were recognized from the western-most Mascota Volcanic Field to the eastern-most Los Tuxtlas Volcanic Field (Ferrari et al., 2005; Ownby et al., 2008; Rodríguez et al., 2010).

Vent clusters allowed Connor (1990) and Mazzarini et al. (2010) to sub-divide the MGVF into four different zones (Fig. 1a), with an average cluster centroid distance of 95 km. The south-western part (~4400 km^2, known as Tancitaro–Nueva Italia region, Fig. 1b; Ownby et al., 2011) comprises the largest (~100 km^3) volcanic centre within this 200 km arc segment (Volcán Tancítaro, Fig. 1b; Ownby et al., 2007; Morelli et al., 2010), and contains 309 monogenetic cones (cinder cone, small shield volcanoes; Ownby et al., 2011) recognized by means of the manual extraction. The volcanic activity in the Tancitaro–Nueva Italia region spans the period of time from 1.2 M.y. until the 1943–1952 eruption of the Paricutin cinder cone (Ban et al., 1992; Pioli et al., 2008; Erlund et al., 2010; Cebriá et al., 2011b; Ownby et al., 2011).

3. Volcanic edifice boundary semiautomatic delimitation

The method, taken into account in this paper, can be applied to any volcano that has a recognizable topographic construct (e.g. a cinder cone) and thus it is not intended for volcanic landforms lacking an edifice such as maars, lava fields or fissure vents (Grosse et al., 2012), However, a recently published similar method has been developed to identify maar volcanoes (the other end of the spectrum, see Seib et al., 2013). The approach used for the computation of DEM-derived morphometric parameters of volcanic edifices comprises: i) DEM (50 × 50 m cell size, digitized from a topographic map at scale 1:50,000) preparation and topographic modeling (i.e. extraction of DEM-derived products); ii) manual boundary delimitation; and iii) computation of the morphometric parameters (basal diameter *Wco*; cone high H; cone slope S; direction of the longest axis). Scoria cone morphometry can be extracted from two freely available DEMs that have almost global coverage: the 90-m Shuttle Radar Topography Mission DEM (SRTM; http://www2.jpl.nasa.gov/srtm) and the 30 m Advanced Spaceborne Thermal Emission and Reflection Radiometer (ASTER) Global DEM (GDEM; http://www.gdem.aster.ersdac.or.jp). Kervyn et al. (2012) showed that the 90-m SRTM DEM (see Fig. 1) is not recommended for small-scale (500 m) and/or steep topographic features. However, medium- to high-resolution DEMs are freely downloadable only for few countries (USA, Italy; Fornaciai et al., 2012 and references therein) and hence a methodology for using low-resolution DEMs is required. We chose a 50 × 50 m DEM resolution mainly because it is an average value between the SRTM-DEM and ASTER-GDEM.

By means of the DEM, the slope and the profile curvature maps were derived. Both products were used for the edifice boundary delimitation, and the slope was also used in the computation of morphometric parameters. As pointed out by Grosse et al. (2012), the profile curvature is the rate of change of slope measured in a vertical plane oriented along the gradient line and thus it directly maps breaks in slope, highlighting both the convexity (positive maxima) and the concavity

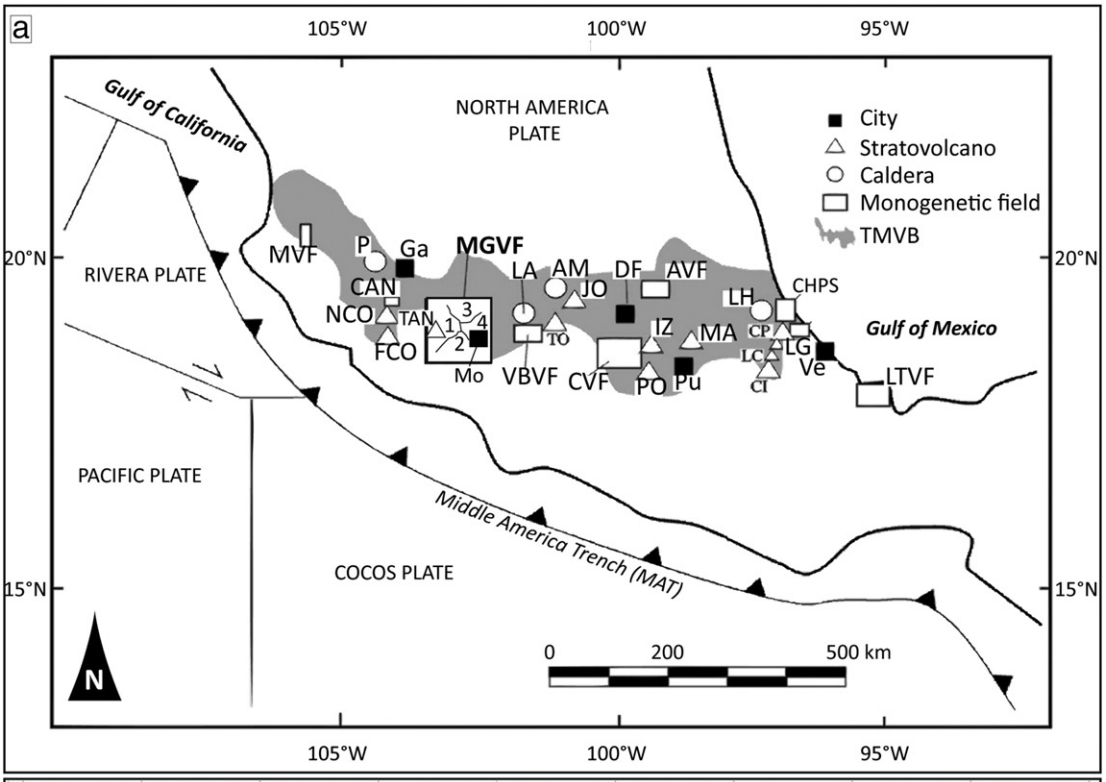
a
105°W
100°W
95°W
20°N
15°N
Gulf of California
NORTH AMERICA PLATE
RIVERA PLATE
PACIFIC PLATE
COCOS PLATE
Middle America Trench (MAT)
Gulf of Mexico
City
Stratovolcano
Caldera
Monogenetic field
TMVB
MVF
P
Ga
MGVF
LA
AM
DF
AVF
CAN
JO
LH
CHPS
NCO
TAN
1
2
3
4
TO
IZ
MA
CP
LC
LG
FCO
Mo
VBVF
CVF
PO
Pu
Ve
CI
LTVF
0
200
500 km
N

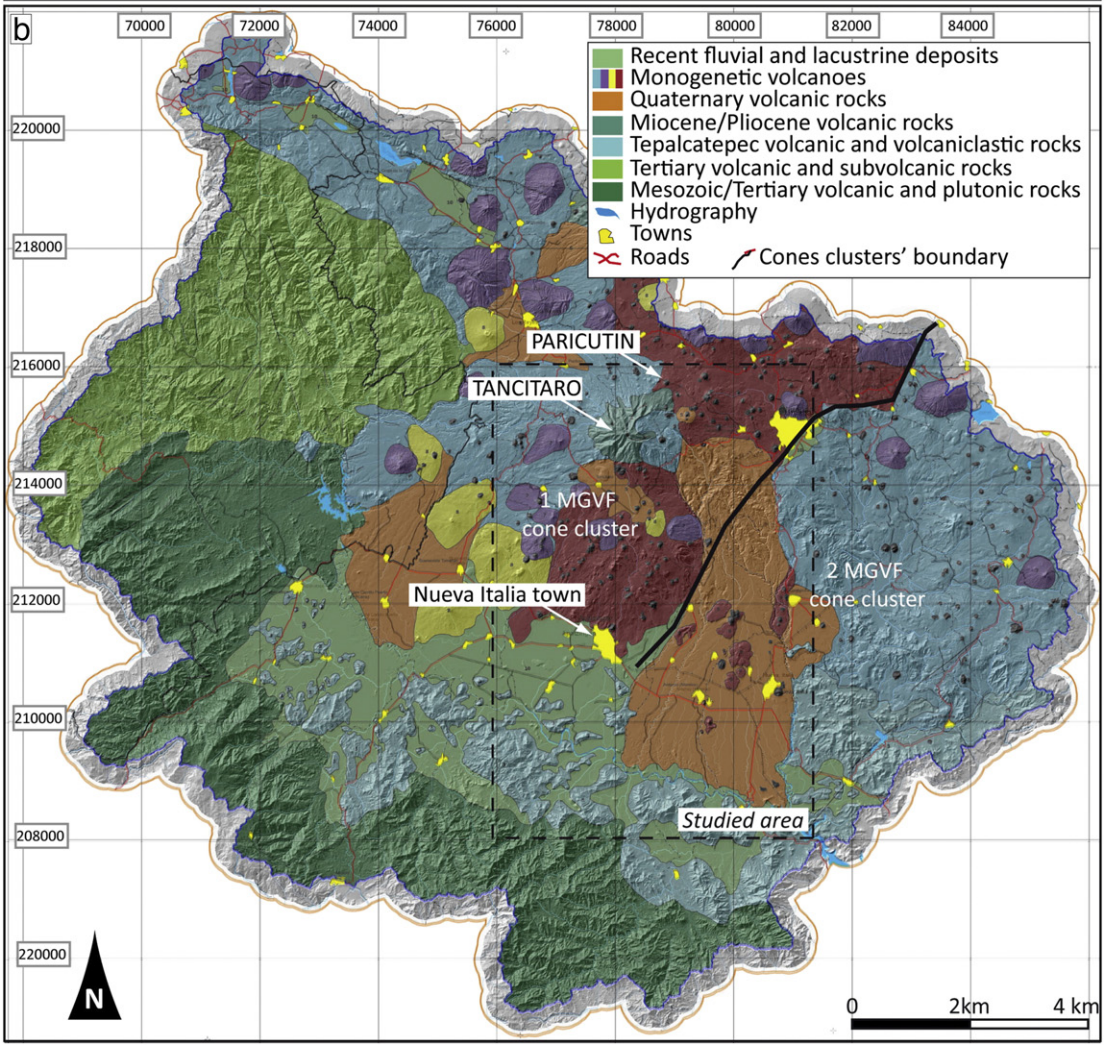
b
70000
72000
74000
76000
78000
80000
82000
84000
220000
218000
216000
214000
212000
210000
208000
220000
Recent fluvial and lacustrine deposits
Monogenetic volcanoes
Quaternary volcanic rocks
Miocene/Pliocene volcanic rocks
Tepalcatepec volcanic and volcaniclastic rocks
Tertiary volcanic and subvolcanic rocks
Mesozoic/Tertiary volcanic and plutonic rocks
Hydrography
Towns
Roads
Cones clusters' boundary
PARICUTIN
TANCITARO
1 MGVF cone cluster
2 MGVF cone cluster
Nueva Italia town
Studied area
N
0
2km
4 km

(negative maxima). The profile curvature and the slope maps were combined in a single data layer (Fig. 2) using the following equation (Grosse et al., 2012)

$$Boundary\ \ delineation\ \ layer = Profile\ \ curvature(norm) * f + Slope(norm) * (1-f) \quad (1)$$

where:

$$Profile\ \ curvature(norm) = \frac{Profile\ \ curvature - Profile\ \ curvature(min)}{Profile\ \ curvature(range)} \quad (2)$$

and:

$$Slope(norm) = \frac{(Slope - Slope(min))^2}{Slope(range)^2} \quad (3)$$

and f is a factor ranging from 0 to 1 that weighs each term and depends on the topography of each particular case (Grosse et al., 2012) In this case, a value of 0.5 is considered to better identify the volcanic boundary because this value provides the best view of the cinder cones. The generated layer is used to trace the boundaries by manually searching for the best path along the minimum values of the generated data layer.

The cinder cone basal diameters have been defined in different ways, as for example by Settle (1979):

$$Wco(settle) = \frac{dmin + dmax}{2} \quad (4)$$

where d_{max} and d_{min} are the maximum and minimum basal diameters of the volcanic edifice, extracted by the convex hull (a polygon generated by connecting the outermost points of the population; Hamilton et al., 2010). We also used the definition of the average *Wco*, as recently redefined by Favalli et al. (2009) as:

$$Wco(Favalli) = \sqrt{\frac{(4\ x\ Aco)}{\pi}} \quad (5)$$

where *Aco* is the planimetric area of the volcanic edifice, including the crater and the outer flanks (Favalli et al., 2009). Moreover, the $Wco_{(Crf)}$, the diameter of a circumference equivalent to the perimeter of a cone (*Crf*), was extracted:

$$Wco(Crf) = \frac{crf}{\pi}. \quad (6)$$

Finally the mean *Wco* was evaluated as:

$$Wco(mean) = \frac{Wco(Settle) + Wco(Favalli)}{2}. \quad (7)$$

The elevation difference between the interpolated DEMs and the basement can be used to define the maximum cone height, *Hmax* (Favalli et al., 2009; Gilichinsky et al., 2010; Rodriguez-Gonzalez et al., 2010; Inbar et al., 2011; Fornaciai et al., 2012; Kervyn et al., 2012; Kereszturi et al., 2013).

The slope has been extrapolated by the DEM and the maximum slope values for each cone have been selected according to Hasenaka and Carmichael (1985).

The crater diameters are hard to measure with accuracy on the low-resolution DEM used in this study (i.e. 50 × 50 m pixel resolution), and are insensitive measures of degradation (Wood, 1980b).

Moreover the cone ellipticity, defined as the ratio between the maximum and the minimum cone diameter (d_{max}/d_{min}), and the trend of the maximum cone axis was extrapolated by the convex hull, giving the information about the influence on the cone morphology and the direction of the feeder dyke, respectively (Tibaldi, 1995; Corazzato and Tibaldi, 2006). Other morphometric parameters conventionally used to detect the orientations of feeder dikes, such as crater elongation, crater rim depression and breaching direction are discarded because: 1) a moderate to high resolution DEM is necessary for the identification of the crater elongation and the crater rim depression; and 2) breaching can coincide with: i) the weakest zone of the edifice, ii) the direction of maximum stress applied to its flanks by magma bulging or fracture propagation (Corazzato and Tibaldi, 2006; Bonali et al., 2011), iii) and landsliding due to steep basal surfaces (Németh et al., 2011). Therefore, breaching could be affected by the lava accumulation or by the flanks bulging rather than by the direction of the feeder dike (Cimarelli et al., 2013; Nolesini et al., 2013). The vent alignments (using the three point alignments method proposed by Le Corvec et al., 2013b) and the vent intensity map (using a search radius of 5 km as proposed by Mazzarini et al., 2010) were also derived from the identified vents. The dimension of the search radius controls the pattern of the intensity distribution. Using r values less than the minimum separation values of vents gives null intensity, while using the maximum distance between the vents as search radius produces a constant intensity distribution (Mazzarini et al., 2010). The use of a search radius about 2–3 times the average separation of vents (2 km) gives optimal results (see Mazzarini et al., 2010 and references therein). As a comparison, a larger search radius (16 km) was used to define the vent clusters of the entire TMVB (Connor, 1990).

Alignment of volcanic centres has been also assessed using the Fry (1979) spatial distribution analysis. This method is used to determine the strain from the distribution of objects (as cracks, minerals, etc) in a rock (Fry, 1979) and preferred orientation of volcanic cone alignments (Kurokawa et al., 1995; Cimarelli et al., 2013).

Comparison between the semi-automatic and the manually extracted results, using the DEM morphology, field observations and available Landsat 7 ETM images (path 028, row 047, cell size 30 m, acquired on 28th November 1999) were also performed. All the DEM analyses were carried out using the ESRI ArcGis 8 software package.

4. Data

4.1. Cone morphometry

The semiautomatic extraction allowed us to identify 137 of the 309 cinder cones identified by the manual extraction (44.3%). At first glance, the main limitation to recognizing more cones with this method is the resolution of the used DEM. Cross checking with LandSat 7 imagery and field validation, testify that the semiautomatic delimitation is not able to identify cones that are too small (d < 500 m), and/or cones located in complicated topography (e.g. upon the Tancitaro debris avalanche, Morelli et al., 2010).

All the calculated *Wco* were used, finding that the $Wco_{(Crf)}$ always has similar values to the $Wco_{(mean)}$, with intermediate values between $Wco_{(Settle)}$ and $Wco_{(Favalli)}$ (Fig. 3a). The *Hmax*/*Wco* ratio varies between 0.139 and 0.146, in good agreement with the results (0.138) of Fornaciai et al. (2012). The *Wco* vs *Hmax* plot (Fig. 3a) shows two different fields, one characterized by higher *Hmax*/*Wco* ratio (0.174) and the other described by a very low ratio (0.080). These two fields are often present

Fig. 1. a) Geographical and geological framework of Mexico showing the distribution of the most important volcanic areas of the Trans-Mexican Volcanic Belt (TMVB). Monogenetic volcanic fields: MVF = Mascota, CAN = Cántaro, MGVF = Michoacán–Guanajuato, VBVF = Valle de Bravo, CVF = Chichinautzin, AVF = Apan, CHPS = Chiconquiaco-Palma Sola, LTVF = Los Tuxtlas. Calderas: P = La Primavera, LA = Los Azufres, AM = Amealco, LH = Los Humeros. Stratovolcanoes: NCO = Nevado de Colima, FCO = Fuego de Colima, TAN = Tancítaro, TO = Nevado de Toluca, JO = Jocotitlán, IZ = Iztaccíhuatl, PO = Popocatépetl, MA = Malinche, CP = Cofre de Perote, LG = La Gloria, LC = Las Cumbres, CI = Citlaltépetl. Cities: Ga = Guadalajara, D.F. = Distrito Federal, Mo = Morelia, Pu = Puebla, Ve = Veracruz (modified after Rodríguez et al., 2010). The location of the four MGVF cone clusters is also reported (Mazzarini et al., 2010). b) Geological map of the Tancitaro–Nueva Italia area (modified after Mendoza et al., 2009).

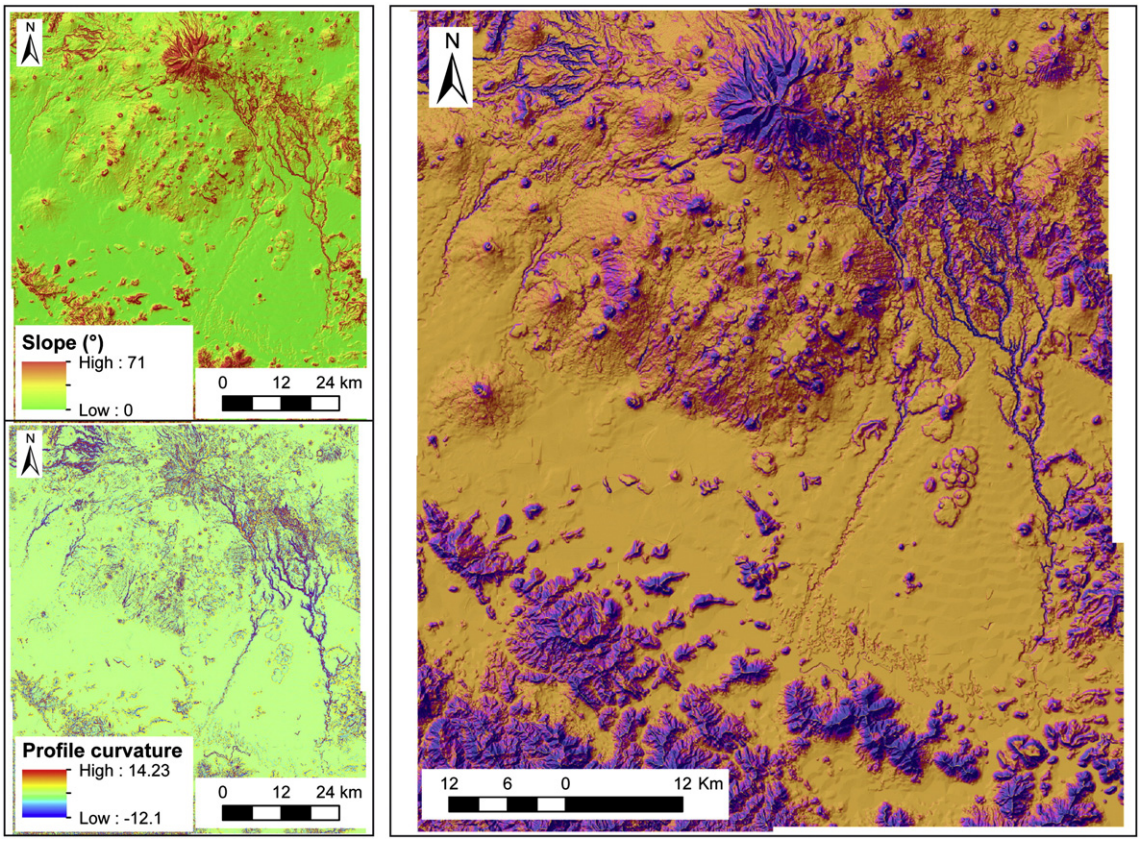

Fig. 2. Semi-automatic cinder cone boundary delineation procedure explanation; a) slope in degrees; b) profile curvature (positive maxima = maximum convexity; negative maxima = maximum concavity); c) boundary delineation map obtained from the combination of a) and b) (see equation in text) that is used to manually trace the cinder cones boundary along the path of minimum values.

in *Hmax/Wco* ratio calculations (Bemis et al., 2011; Kervyn et al., 2012; Rodriguez-Gonzalez et al., 2012; Kereszturi et al., 2013) and may be associated with different eruptive styles prevailing during the formation of the cone (Hawaiian vs Strombolian or Violent Strombolian, see Martin and Németh, 2006; Cimarelli et al., 2013). While the high *Hmax/Wco* ratio is generally related to young, poorly eroded cinder cones (Favalli et al., 2009; Inbar et al., 2011), the low *Hmax/Wco* ratio could be related to several factors: 1) eroded cones (Wood, 1980b; Bemis et al., 2011); 2) influence on the eruptive style and/or the change in vent location (Kervyn et al., 2012); 3) difficulty in extrapolating the actual *Hmax* with the semi-automatic procedure due to slope breaks within cones at high gradients or disturbance of slope breaks from neighboring landforms, as with lava flow accumulation at the cone base (Euillades et al., 2013). The *Hmax/Wco* ratio and *S* have been plotted (Fig. 3c) and a clear relationship is evident between slope and *Hmax/Wco*, according to Wood (1980a) and Inbar et al. (2011) for Etna (Italy), Tolbachik (Kamchtka) and San Francisco Volcanic Field (Arizona, USA).

4.2. Alignments and vent distribution

The directions of three point cinder cone alignments (manual and semiautomatic extracted), the convex hull major axis (only semiautomatic extracted) and the cone elongations (manual and semiautomatic extracted) of the entire Tancitaro–Nueva Italia region where plotted in a rose diagram (Fig. 4) and the alignment of volcanic centres has also been assessed using Fry (1979) spatial distribution analysis. The cinder cone ellipticity is very low (Fig. 4) and therefore no statistically significant information on the mean feeder dikes geometry could be extrapolated from the strike of the maximum cone elongations. For comparison, cone elongation has been manually extrapolated by integrating the DEM and the LandSat 7 imagery. The cones with evident elongation numbered only 35, but a slight directionality of the cone elongation has been found, with a mean direction of N208°. Semiautomatically extracted (N224°) and manually extracted (N191°) vent alignments show evident NE–SW directionality (Fig. 4). The results of the Fry plots show similar NE-striking σ_{max}, with an average error of 20–30% in the result (Dunne et al., 1990). This is coherent with the main alignment direction in the southern sector of the MGVF recognized by Wadge and Cross (1988), Connor (1990), Kurokawa et al. (1995) and Cebriá et al. (2011a).

We also analyze the intensity of vents distribution (Fig. 5) computing the number of vents within a radius *r* centred on each vent of the data set (function Point Density of ArcGis 8). The dimension of the search radius strongly controls the final pattern of the intensity distribution; the higher the r value the smoother is the pattern (Connor, 1990; Lutz and Gutmann, 1995; Mazzarini et al., 2010; Germa et al., 2013). The *r* value of 5 km proposed by Mazzarini et al. (2010) for the entire MGVF was used, being the largest value for the vent spacing. Obviously, the maximum number of cones in a cell changes dependent upon the manual and the semiautomatic extraction but both vent intensity maps show several maxima, one located to the NW with respect to the Volcano Tancitaro, one to the NE, one to the S and another one located at the SE boundary of the studied area. The mean distance between the centroid of each maximum is 24 km.

5. Discussions

5.1. Comparison between manual and semiautomatic procedure

We chose to compare parameters derived from the semiautomatic procedure with the manual-extracted cones using the $Wco_{(Crf)}$, being also the most easy to derive from the DEM. In general, *Wco* is the

more stable parameter over time, changing in a similar way for all the cinder cones, during the eruption phase, the cone growth and the post-eruption erosion process (Pérez-López et al., 2011). In fact, the *Wco* is less affected the parameters by erosion and mass transport (Wood, 1980b). Recent cones (0–0.05 My. old) have stable *Wco* value, while degradation due to weathering of material from the summit of a cone and mass wasting redistributes the material around the flanks (Wood, 1980b). This phenomenon is able to modify cones with *Wco* values larger than initial values (0.05–3 My old cones; Wood, 1980b).

The comparison was made on cinder cones located north of the Volcano Tancitaro, where the Paricutin cinder cone is located. The *Hmax/Wco* ratios are very similar between the semi-automatic (0.1586, $R^2 = 0.4393$) and the manual (0.1618, $R^2 = 0.2376$) extraction (Fig. 3b).

The power-law for the *Wco*-distribution of the cinder cones of the Tancitaro–Nueva Italia region is very similar to the one of the entire MGVF. Considering a log–log relationship as proposed by Pérez-López et al. (2011) for the scaling lows of the size-distribution of cinder cones in monogenetic volcanic fields, the *Wco* threshold is 1.35 km for the 137 semi-automatic extracted cones and the power low size-distribution have the inner and outer cut-off at 0.9 and 1.4 km, respectively. For comparison, the same values for the entire MGVF are 1.3 km (*Wco* threshold), 0.7 km (inner cut-off) and 3 (outer cut-off), for a total number of 954 cones (Pérez-López et al., 2011). This would imply a good correlation between the *Wco* derived from the semi-automatic extraction and the manual extraction made by Pérez-López et al. (2011).

5.2. Cinder cone alignments and vent intensity maps: implication for the tectonic control on volcanism

The persistency of NE–SW vent alignments and manually extracted cone elongations in the Tancitaro–Nueva Italia region (Fig. 4) allows us to identify a NE–SW maximum principal compressive stress (σ_{max}) and a NW-SE minimum principal compressive stress (σ_{min}, Fig. 4). These results are the same of Connor (1990), Kurokawa et al. (1995) and Cebriá et al. (2011a), and NE–SW striking lineaments are observed in pre-Miocene rocks and beneath the Plio-Quaternary volcanic cover of the MGVF as inferred from the geophysical data (Pacheco et al., 1999; Gardine et al., 2011).

The central, NE and NW vent intensity maxima recognized in this work correspond to one of the four vent intensity maxima present within the whole MGVF (Mazzarini et al., 2010). The other vent intensity maximum identified here (in the south-easternmost part of the study area) is related to another area identified by Mazzarini et al. (2010), where the 1759–1766 Jorullo cinder cone is located (Guilbaud et al., 2011). The average distance *d* between the centroids is 24 km. Vent spacing can be considered in relation to the energy available to the system (i.e., the buoyancy of a batch of magma) and the critical energy necessary to allow the initial mobilization of magma, which in turn relates to the thickness of the overlying crust (Turcotte and Schubert, 2002; Lesti et al., 2008).

Applying the Turcotte and Schubert (2002) relationship:

$$d = 2.568h \tag{8}$$

to the Tancitaro–Nueva Italia region, the depth *h* of the magma reservoirs is determined as 9–10 km. This depth corresponds to the shallower depth of crustal assimilation and melt inclusions CO_2 entrapment of the Paricutin magma (Luhr, 2001; Cebriá et al., 2011b). Based on the reconstruction of Pioli et al. (2009) and Erlund et al. (2010), the Paricutin magma rose from the crustal level (14 km below the vent) and experienced different phenomena of magma crystallization and vesiculation during its path toward the surface. Moreover, the depth of 9 km is the depth origin of the 2006 dike intrusion beneath the NW vent intensity maxima (Fig. 5; Gardine et al., 2011). This event was characterized by the upward location of the hypocentres from 9 km to 4–5 km depth, that correspond to an initial migration

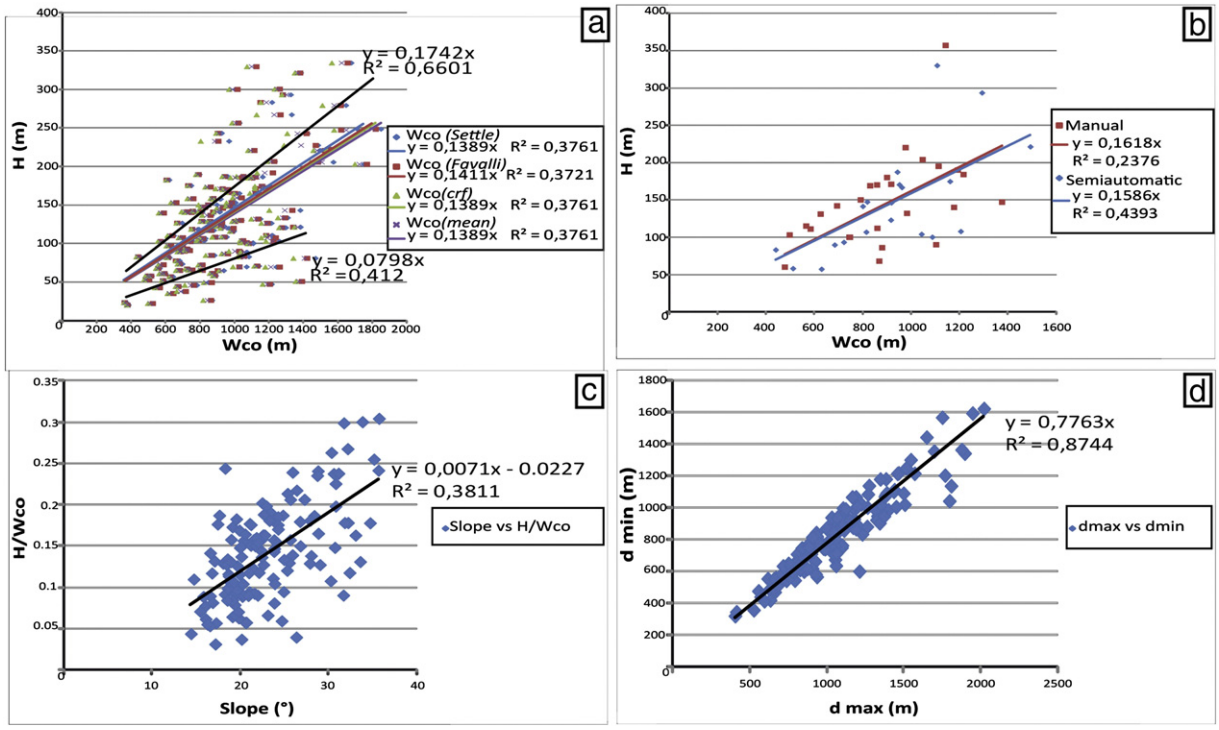

Fig. 3. Graph showing the relationship between various morphometric parameters: a) *Wco* vs *Hmax* for the semi-automatic extracted cones (*Wco* is based on Eqs. (4), (5), (6) and (7)); b) comparison between *Wco* vs *Hmax* for selected cones (*Wco* is based on Eq. (7)); c) slope vs *Hmax/Wco* ratio for the semi-automatic extracted cones (*Wco* is based on Eq. (7)); d_{min} vs d_{max} based on the convex hull for the semi-automatic extracted cones.

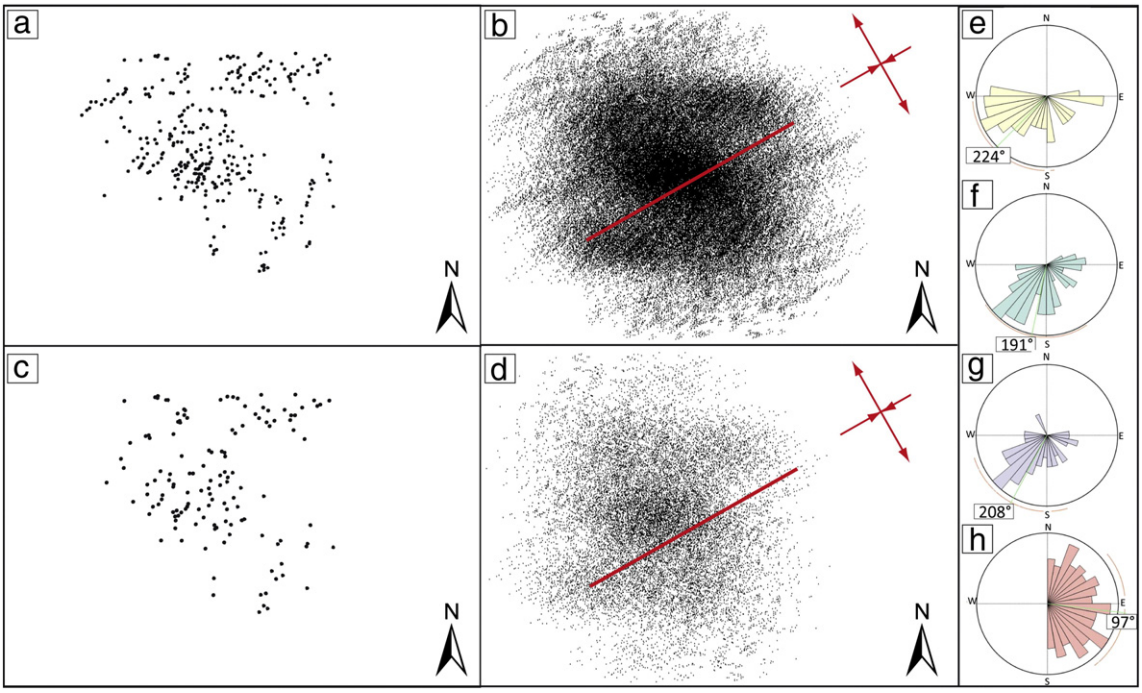

Fig. 4. a) Manually extracted vents; b) Fry (1979) plot describing the spatial distribution of the cones, their preferential alignments (red line) and the orientation of the stress tensor (arrows) based on a); c) semi-automatic extracted vent; d) Fry (1979) plot describing the spatial distribution of the cones, their preferential alignments (red line) and the orientation of the stress tensor (arrows) based on c); e) rose diagrams of the vent alignments based on a); f) rose diagrams of the vent alignments based on c); g) rose diagrams of the cone elongation (as defined by Tibaldi, 1995); h) rose diagrams of the azimuth of the maximum basal diameter (convex hull).

towards the northeast followed by a progressive movement toward the southwest (Gardine et al., 2011). The 2006 volcanotectonic seismic swarm that accompanied the dike intrusion was aligned in a NE–SW direction similar to the 1997 swarm (Pacheco et al., 1999), both with epicentres located within 10 km. The 4–5 km depth corresponds to the temporary storage and crystallization of the Parícutin magma within a shallow dike and sill complex during the late phase of the eruption (Erlund et al., 2010).

Summarizing, the recent volcanism in the Tancitaro–Nueva Italia region was fed by basaltic magma originated at great depth (37 km; Mazzarini et al., 2010), residing at crustal level (10–14 km; Erlund et al., 2010; Cebriá et al., 2011b). It rose fracturing the crust and forming dikes from 9 to 10 km (based on the Gardine et al., 2011 seismic data and the vent intensity map proposed here) with a main NE–SW direction (based on the Gardine et al., 2011 seismic data and the vent alignments by Connor, 1990; Kurokawa et al., 1995; Cebriá et al., 2011a and

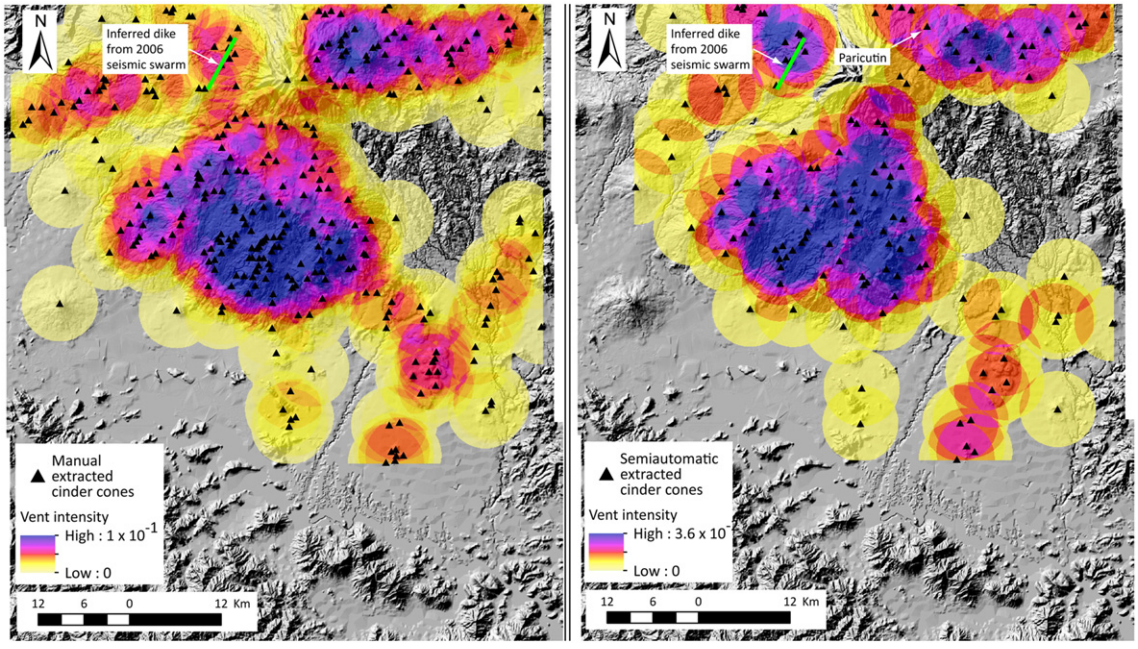

Fig. 5. a) Manually extracted and b) semi-automatically extracted vent intensity maps. In both maps the approximate location of the 2006 intruded dike is based on the double-difference relocated epicenters (Gardine et al., 2011).

the data proposed here) and in part resided at shallower level forming sill-like bodies (~4 km; Pioli et al., 2009; Erlund et al., 2010; Gardine et al., 2011).

6. Conclusions

In this work the semi-automatic delimitation of a volcanic edifice boundary proposed by Grosse et al. (2009, 2012) for stratovolcanoes was tested on cinder cones. This method, based on the integration of the DEM-derived slope and curvature maps, has been applied to the Tancitaro–Nueva Italia region (part of the Michoacán–Guanajuato Volcanic Field, Mexico), where there are 309 Plio-Quaternary cinder cones.

Considering these morphologic features, the semiautomatic extraction allowed the identification of 137 of the 309 cinder cones previously recognized from manual extraction. This value corresponds to the 44.3% of the total number. The comparison between the semiautomatic procedure with the manual-extracted cones and literature data (mainly considering the cone basal diameter, *Wco*) revealed a good correlation between the *Wco* derived from the semi-automatic extraction and that from manual extraction.

The integration of the semiautomatic cinder cone extraction with literature data allowed us to summarize the recent volcanism in the Tancitaro–Nueva Italia region. The persistency of NE–SW vent alignments and cone elongations in the studied region suggest a NE–SW σ_{max} and a NW–SE σ_{min}, in accordance with already published data (Connor, 1990; Kurokawa et al., 1995; Cebriá et al., 2011a).

From the vent intensity maps based on both the manual and semiautomatic cinder cone extraction we derived four vent intensity maxima, one located to the NW with respect to the Tancitaro Volcano, one to the NE, one to the S and another vent cluster located at the SE boundary of the studied area. The mean distance between the centroid of each cluster is 24 km, corresponding to a magma reservoir depth at 9–10 km.

Acknowledgments

The present work is one of the results born from the collaborative relationship between the Department of Earth Sciences, University of Firenze and the Instituto de Investigaciones Metalúrgicas, Universidad Michoacana de San Nicolás de Hidalgo, officially ratified by a bilateral agreement on cultural cooperation between Universities in the field of natural hazards. FeDiT is supported by a post-doc fellowship founded by the Regione Toscana (UNIPI-FSE) under the project RADSAFE (UNIPI-4) in the framework of the research agreement between DST-UNIPI, DST-UNIFI and Ellegi-Lisalab. The authors are grateful to K. Németh and an anonymous reviewer for precious suggestions and comments that significantly improved the manuscript. A. Plater is acknowledged for the editorial handling of this manuscript.

References

Andronico, D., Cristaldi, A. Del, Carlo, P., Taddeucci, J., 2009. Shifting styles of basaltic explosive activity during the 2002–03 eruption of Mt. Etna, Italy. J. Volcanol. Geotherm. Res. 180, 110–122.

Ban, M., Hasenaka, T., Delgado, H., Takaoka, N., 1992. K–Ar ages of lavas from shield volcanoes in Michoacán–Guanajuato, Mexico. Geofis. Int. 31 (4), 467–473.

Beggan, C., Hamilton, C.W., 2010. New image processing software for analyzing object size-frequency distribution, geometry, orientation, and spatial distribution. Comput. Geosci. 36, 539–549.

Bemis, K., Walker, J., Borgia, A., Turrin, B., Neri, M., Swisher III, C., 2011. The growth and erosion of cinder cones in Guatemala and El Salvador: models and statistics. J. Volcanol. Geotherm. Res. 201, 39–52.

Bohnenstiehl, D.R., Howell, J.K., White, S.M., Hey, R.N., 2012. A modified basal outlining algorithm for identifying topographic highs from gridded elevation data, part 1: motivation and methods. Comput. Geosci. 49, 308–314.

Bonali, F., Corazzato, C., Tibaldi, A., 2011. Identifying rift zones on volcanoes: an example from La Réunion Island, Indian Ocean. Bull. Volcanol. 73, 347–366.

Brenna, M., Cronin, S.J., Németh, K., Smith, I.E.M., Sohn, Y.K., 2011. The influence of magma plumbing complexity on monogenetic eruptions, Jeju Island, Korea. Terra Nova 23 (2), 70–75.

Broz, P., Hauber, E., 2012. A unique volcanic field in Tharsis, Mars: pyroclastic cones as evidence for explosive eruptions. Icarus 218, 88–99.

Cebriá, J.M., Martín-Escorza, C., López-Ruiz, J., Morán-Zenteno, D.J., Martiny, B.M., 2011a. Numerical recognition of alignments in monogenetic volcanic areas: examples from the Michoacán–Guanajuato Volcanic Field in Mexico and Calatrava in Spain. J. Volcanol. Geotherm. Res. 201, 73–82.

Cebriá, J.M., Martiny, B.M., López-Ruiz, J., Morán-Zenteno, D.J., 2011b. The Parícutin calcalkaline lavas: new geochemical and petrogenetic modelling constraints on the crustal assimilation process. J. Volcanol. Geotherm. Res. 201, 113–125.

Cimarelli, C., Di Traglia, F., Taddeucci, J., 2010. Basaltic scoria textures from a zoned conduit as precursors to violent Strombolian activity. Geology 38, 439–442.

Cimarelli, C., Di Traglia, F., de Rita, D., Fernandez Turriel, J-.L., Torrente, D.G., 2013. Space–time evolution of monogenetic volcanism in the mafic Garrotxa Volcanic Field (NE Iberian Peninsula). Bull. Volcanol. 75, 1–18.

Connor, C.B., 1987. Structure of the Michoacán–Guanajuato volcanic field, Mexico. J. Volcanol. Geotherm. Res. 33, 191–200.

Connor, C.B., 1990. Cinder cone clustering in the TransMexican Volcanic Belt: implications for structural and petrologic models. J. Geophys. Res. Solid Earth (1978–2012) 95 (B12), 19395–19405.

Connor, C.B., Stamatakos, J.A., Ferrill, D.A., Hill, B.E., Ofoegbu, G.I., Conway, F.M., Trapp, J., 2000. Geologic factors controlling patterns of small-volume basaltic volcanism: application to a volcanic hazards assessment at Yucca Mountain, Nevada. J. Geophys. Res. 105 (B1), 417–432.

Corazzato, C., Tibaldi, A., 2006. Fracture control on type, morphology and distribution of parasitic volcanic cones: an example from Mt. Etna, Italy. J. Volcanol. Geotherm. Res. 158, 177–194.

Di Traglia, F., Cimarelli, C., De Rita, D., Gimeno Torrente, D., 2009. Changing eruptive styles in basaltic explosive volcanism: examples from Croscat complex scoria cone, Garrotxa Volcanic Field (NE Iberian Peninsula). J. Volcanol. Geotherm. Res. 180, 89–109.

Di Traglia, F., Pistolesi, M., Rosi, M., Bonadonna, C., Fusillo, R., Roverato, M., 2013. Growth and erosion: the volcanic geology and morphological evolution of La Fossa (Island of Vulcano, Southern Italy) in the last 1000 years. Geomorphology 194, 94–107.

Dóniz, J., Romero, C., Coello, E., Guillén, C., Sánchez, N., García-Cacho, L., García, A., 2008. Morphological and statistical characterisation of recent mafic volcanism on Tenerife (Canary Islands, Spain). J. Volcanol. Geotherm. Res. 173, 185–195.

Dunne, W.M., Onasch, C.M., Williams, R.T., 1990. The problem of strain-marker centers and the Fry method. J. Struct. Geol. 12, 933–938.

Erlund, E.J., Cashman, K.V., Wallace, P.J., Pioli, L., Rosi, M., Johnson, E., Granados, H.D., 2010. Compositional evolution of magma from Parícutin Volcano, Mexico: the tephra record. J. Volcanol. Geotherm. Res. 197, 167–187.

Euillades, L.D., Grosse, P., Euillades, P.A., 2013. NETVOLC: an algorithm for automatic delimitation of volcano edifice boundaries using DEMs. Comput. Geosci. 56, 151–160.

Favalli, M., Karátson, D., Mazzarini, F., Pareschi, M.T., Boschi, E., 2009. Morphometry of scoria cones located on a volcano flank: a case study from Mt. Etna (Italy), based on high-resolution LiDAR data. J. Volcanol. Geotherm. Res. 186, 320–330.

Ferrari, L., Tagami, T., Eguchi, M., Orozco-Esquivel, M.T., Petrone, C.M., Jacobo-Albarrán, J., López-Martínez, M., 2005. Geology, geochronology and tectonic setting of late Cenozoic volcanism along the southwestern Gulf of Mexico: the Eastern Alkaline Province revisited. J. Volcanol. Geotherm. Res. 146, 284–306.

Fornaciai, A., Behncke, B., Favalli, M., Neri, M., Tarquini, S., Boschi, E., 2010. Detecting short-term evolution of Etnean cinder cones: a LIDAR-based approach. Bull. Volcanol. 72, 1209–1222.

Fornaciai, A., Favalli, M., Karátson, D., Tarquini, S., Boschi, E., 2012. Morphometry of scoria cones, and their relation to geodynamic setting: a DEM-based analysis. J. Volcanol. Geotherm. Res. 217, 56–72.

Fry, N., 1979. Random point distributions and strain measurement in rocks. Tectonophysics 60, 89–105.

Gaffney, E.S., Damjanac, B., 2006. Localization of volcanic activity: topographic effects on dike propagation, eruption and conduit formation. Geophys. Res. Lett. 33, L14313.

Gaffney, E.S., Damjanac, B., Valentine, G.A., 2007. Localization of volcanic activity: 2. Effects of pre-existing structure. Earth Planet. Sci. Lett. 263, 323–338.

Gardine, M., West, M.E., Cox, T., 2011. Dike emplacement near Parícutin volcano, Mexico in 2006. Bull. Volcanol. 73, 123–132.

Germa, A., Connor, L.J., Cañon-Tapia, E., Le Corvec, N., 2013. Tectonic and magmatic controls on the location of post-subduction monogenetic volcanoes in Baja California, Mexico, revealed through spatial analysis of eruptive vents. Bull. Volcanol. 75, 1–14.

Gilichinsky, M., Melnikov, D., Melekestsev, I., Zaretskaya, N., Inbar, M., 2010. Morphometric measurements of cinder cones from digital elevation models of Tolbachik volcanic field, central Kamchatka. Can. J. Remote. Sens. 36, 287–300.

Gómez-Tuena, A., Langmuir, C.H., Goldstein, S.L., Straub, S.M., Ortega-Gutiérrez, F., 2007. Geochemical evidence for slab melting in the Trans-Mexican Volcanic Belt. J. Petrol. 48, 537–562.

Grosse, P., De Vries, B.V.W., Petrinovic, I.A., Euillades, P.A., Alvarado, G.E., 2009. Morphometry and evolution of arc volcanoes. Geology 37, 651–654.

Grosse, P., van Wyk de Vries, B., Euillades, P.A., Kervyn, M., Petrinovic, I.A., 2012. Systematic morphometric characterization of volcanic edifices using digital elevation models. Geomorphology 136, 114–131.

Guilbaud, M.N., Siebe, C., Layer, P., Salinas, S., Castro-Govea, R., Garduño Monroy, V.H., Le Corvec, N., 2011. Geology, geochronology, and tectonic setting of the Jorullo volcano region, Michoacán, México. J. Volcanol. Geotherm. Res. 201, 97–112.

Hamilton, C.W., Fagents, S.A., Thordarson, T., 2010. Explosive lava–water interactions II: self-organization processes among volcanic rootless eruption sites in the 1783–1784 Laki lava flow, Iceland. Bull. Volcanol. 72, 469–485.

Hasenaka, T., Carmichael, I.S., 1985. The cinder cones of Michoacán–Guanajuato, central Mexico: their age, volume and distribution, and magma discharge rate. J. Volcanol. Geotherm. Res. 25, 105–124.

Head III, J.W., Wilson, L., 1989. Basaltic pyroclastic eruptions: influence of gas-release patterns and volume fluxes on fountain structure, and the formation of cinder cones, spatter cones, rootless flows, lava ponds and lava flows. J. Volcanol. Geotherm. Res. 37, 261–271.
Howell, J.K., White, S.M., Bohnenstiehl, D.R., 2012. A modified basal outlining algorithm for identifying topographic highs in gridded elevation data, part 2: application to Springerville Volcanic Field. Comput. Geosci. 49, 315–322.
Inbar, M., Gilichinsky, M., Melekestsev, I., Melnikov, D., Zaretskaya, N., 2011. Morphometric and morphological development of Holocene cinder cones: a field and remote sensing study in the Tolbachik volcanic field, Kamchatka. J. Volcanol. Geotherm. Res. 201, 301–311.
Kereszturi, G., Németh, K., 2012. Monogenetic basaltic volcanoes: genetic classification, growth, geomorphology and degradation. In: Németh, K. (Ed.), Updates in Volcanology — New Advances in Understanding Volcanic Systems. InTech, Rijeka, Croatia. http://dx.doi.org/10.5772/51387.
Kereszturi, G., Jordan, G., Németh, K., Dóniz-Páez, J.F., 2012. Syn-eruptive morphometric variability of monogenetic scoria cones. Bull. Volcanol. 74 (9), 2171–2185.
Kereszturi, G., Geyer, A., Martí, J., Németh, K., Dóniz-Páez, F.J., 2013. Evaluation of morphometry-based dating of monogenetic volcanoes — a case study from Bandas del Sur, Tenerife (Canary Islands). Bull. Volcanol. 75, 1–19.
Kervyn, M., Ernst, G.G.J., Carracedo, J.C., Jacobs, P., 2012. Geomorphometric variability of "monogenetic" volcanic cones: evidence from Mauna Kea, Lanzarote and experimental cones. Geomorphology 136, 59–75.
Kurokawa, K., Otsuki, K., Hasenaka, T., 1995. Tectonic stress field and fractal distribution of volcanoes in the Michoacán–Guanajuato region of the Mexican Volcanic Belt. Geofís. Int. 34, 309–320.
Le Corvec, N., Spörli, K.B., Rowland, J., Lindsay, J., 2013a. Spatial distribution and alignments of volcanic centers: clues to the formation of monogenetic volcanic fields. Earth Sci. Rev. 124, 96–114.
Le Corvec, N., Bebbington, M.S., Lindsay, J.M., McGee, L.E., 2013b. Age, distance, and geochemical evolution within a monogenetic volcanic field: analyzing patterns in the Auckland Volcanic Field eruption sequence. Geochem. Geophys. Geosyst. 14, 3648–3665.
Le Corvec, N., Menand, T., Lindsay, J., 2013c. Interaction of ascending magma with pre-existing crustal fractures in monogenetic basaltic volcanism: an experimental approach. J. Geophys. Res. Solid Earth 118, 968–984.
Lesti, C., Giordano, G., Salvini, F., Cas, R., 2008. Volcano tectonic setting of the intraplate, Pliocene–Holocene, Newer Volcanic Province (southeast Australia): role of crustal fracture zones. J. Geophys. Res. Solid Earth (1978–2012) 113 (B7).
Luhr, J.F., 2001. Glass inclusions and melt volatile contents at Paricutin Volcano, Mexico. Contrib. Mineral. Petrol. 142, 261–283.
Lutz, T.M., Gutmann, J.T., 1995. An improved method for determining and characterizing alignments of pointlike features and its implications for the Pinacate volcanic field, Sonora, Mexico. J. Geophys. Res. 100 (B9), 17659–17670.
Martin, U., Németh, K., 2006. How Strombolian is a "Strombolian" scoria cone? Some irregularities in scoria cone architecture from the Transmexican Volcanic Belt, near Volcán Ceboruco, (Mexico) and Al Haruj (Libya). J. Volcanol. Geotherm. Res. 155, 104–118.
Mazzarini, F., Ferrari, L., Isola, I., 2010. Self-similar clustering of cinder cones and crust thickness in the Michoacán–Guanajuato and Sierra de Chichinautzin volcanic fields, Trans-Mexican Volcanic Belt. Tectonophysics 486, 55–64.
Mendoza, M.E., Toledo, A., Velázquez, A., Garduño, V.H., Plascencia, H., 2009. Regionalización fisicogeográfica. In: Mendoza, M.E., Velázquez, A., Larrazábal, A., Toledo, A. (Eds.), Atlas Fisicogeográfico de la Cuenca del Río Tepalcatepec. Instituto Nacional de Ecología, SEMARNAT and Colegio de Michoacán, pp. 15–27.
Morelli, S., Garduño Monroy, V.H., Gigli, G., Falorni, G., Rocha, E.A., Casagli, N., 2010. The Tancitaro debris avalanche: characterization, propagation and modeling. J. Volcanol. Geotherm. Res. 193, 93–105.
Németh, K., Risso, C., Nullo, F., Kereszturi, G., 2011. The role of collapsing and cone rafting on eruption style changes and final cone morphology: Los Morados scoria cone, Mendoza, Argentina. Cent. Eur. J. Geosci. 3 (2), 102–118.
Nolesini, T., Di Traglia, F., Del Ventisette, C., Moretti, S., Casagli, N., 2013. Deformations and slope instability on Stromboli volcano: integration of GBInSAR data and analogue modeling. Geomorphology 180–181, 242–254.
Ownby, S., Delgado Granados, H., Lange, R.A., Hall, C.M., 2007. Volcan Tancitaro, Michoacán, Mexico, $^{40}Ar/^{39}Ar$ constraints on its history of sector collapse. J. Volcanol. Geotherm. Res. 161, 1–14.
Ownby, S.E., Lange, R.A., Hall, C.M., 2008. The eruptive history of the Mascota volcanic field, western Mexico: age and volume constraints on the origin of andesite among a diverse suite of lamprophyric and calc-alkaline lavas. J. Volcanol. Geotherm. Res. 177, 1077–1091.
Ownby, S.E., Lange, R.A., Hall, C.M., Delgado-Granados, H., 2011. Origin of andesite in the deep crust and eruption rates in the Tancítaro–Nueva Italia region of the central Mexican arc. Geol. Soc. Am. Bull. 123, 274–294.
Pacheco, J.F., Valdés-González, C., Delgado, H., Singh, S.K., Zuñiga, F.R., Mortera-Gutiérrez, C.A., Santoyo, M.A., Domìnguez, J., Barrón, R., 1999. Tectonic implications of the earthquake swarm of 1997 in the Michoacán Triangle, Mexico. J. S. Am. Earth Sci. 12, 567–577.
Parfitt, E.A., 2004. A discussion of the mechanisms of explosive basaltic eruptions. J. Volcanol. Geotherm. Res. 134, 77–107.
Pasquare, G., Garduño Monroy, V.H., Tibaldi, A., Ferrari, L., 1990. Migrazione di un arco vulcanico continentale: Dalla Sierra Madre Occidentale all "arco Vulcanico Messiano". Mem. Soc. Geol. Ital. 45, 939–946.
Pasquarè, G., Ferrari, L., Garduño Monroy, V.H., Tibaldi, A., Vezzoli, L., 1991. Geologic map of the central Mexican Volcanic Belt, states of Guanajuato and Michoacán, Mexico. University of Milano, Geological Society of America, Map and Chart Series MCH072.
Pérez-López, R., Legrand, D., Garduño Monroy, V.H., Rodríguez-Pascua, M.A., Giner-Robles, J.L., 2011. Scaling laws of the size-distribution of monogenetic volcanoes within the Michoacán–Guanajuato Volcanic Field (Mexico). J. Volcanol. Geotherm. Res. 201, 65–72.
Pioli, L., Erlund, E., Johnson, E., Cashman, K., Wallace, P., Rosi, M., Delgado Granados, H., 2008. Explosive dynamics of violent Strombolian eruptions: the eruption of Parícutin Volcano 1943–1952 (Mexico). Earth Planet. Sci. Lett. 271, 359–368.
Pioli, L., Azzopardi, B.J., Cashman, K.V., 2009. Controls on the explosivity of scoria cone eruptions: magma segregation at conduit junctions. J. Volcanol. Geotherm. Res. 186, 407–415.
Rodríguez, S.R., Morales-Barrera, W., Layer, P., González-Mercado, E., 2010. A quaternary monogenetic volcanic field in the Xalapa region, eastern Trans-Mexican volcanic belt: geology, distribution and morphology of the volcanic vents. J. Volcanol. Geotherm. Res. 197, 149–166.
Rodriguez-Gonzalez, A., Fernandez-Turiel, J.L., Perez-Torrado, F.J., Gimeno, D., Aulinas, M., 2010. Geomorphological reconstruction and morphometric modelling applied to past volcanism. Int. J. Earth Sci. 99, 645–660.
Rodriguez-Gonzalez, A., Fernandez-Turiel, J.L., Perez-Torrado, F.J., Paris, R., Gimeno, D., Carracedo, J.C., Aulinas, M., 2012. Factors controlling the morphology of monogenetic basaltic volcanoes: the Holocene volcanism of Gran Canaria (Canary Islands, Spain). Geomorphology 136, 31–44.
Rubin, A.M., 1995. Propagation of magma-filled cracks. Annu. Rev. Earth Planet. Sci. 23, 287–336.
Seib, N., Kley, J., Buchel, G., 2013. Identification of maars and similar volcanic landforms in the West Eifel Volcanic Field through image processing of DTM data: efficiency of different methods depending on preservation state. Int. J. Earth Sci. 102 (3), 875–901.
Settle, M., 1979. The structure and emplacement of cinder cone fields. Am. J. Sci. 279, 1089–1107.
Spudis, P.D., McGovern, P.J., Kiefer, W.S., 2013. Large shield volcanoes on the Moon. J. Geophys. Res. Planets 118, 1063–1081.
Taddeucci, J., Pompilio, M., Scarlato, P., 2004. Conduit processes during the July–August 2001 explosive activity of Mt. Etna (Italy): inferences from glass chemistry and crystal size distribution of ash particles. J. Volcanol. Geotherm. Res. 137, 33–54.
Takada, A., 1994. The influence of regional stress and magmatic input on styles of monogenetic and polygenetic volcanism. J. Geophys. Res. Solid Earth (1978–2012) 99, 13563–13573.
Tibaldi, A., 1995. Morphology of pyroclastic cones and tectonics. J. Geophys. Res. Solid Earth (1978–2012) 100 (B12), 24521–24535.
Turcotte, D.L., Schubert, G., 2002. Geodynamics. Cambridge University Press, New York 0-521-66624-4 (456 pp.).
Valentine, G.A., Gregg, T.K.P., 2008. Continental basaltic volcanoes — processes and problems. J. Volcanol. Geotherm. Res. 177, 857–873 (1-31).
Valentine, G.A., Krogh, K.E., 2006. Emplacement of shallow dikes and sills beneath a small basaltic volcanic center — the role of pre-existing structure (Paiute Ridge, southern Nevada, USA). Earth Planet. Sci. Lett. 246, 217–230.
Valentine, G.A., Perry, F.V., 2007. Tectonically controlled, time-predictable basaltic volcanism from a lithospheric mantle source (central Basin and Range Province, USA). Earth Planet. Sci. Lett. 261, 201–216.
Valentine, G.A., Krier, D., Perry, F.V., Heiken, G., 2005. Scoria cone construction mechanisms, Lathrop Wells volcano, southern Nevada, USA. Geology 33, 629–632.
Wadge, G., Cross, A., 1988. Quantitative methods for detecting aligned points: an application to the volcanic vents of the Michoacán–Guanajuato volcanic field, Mexico. Geology 16, 815–818.
Wood, C.A., 1980a. Morphometric evolution of cinder cones. J. Volcanol. Geotherm. Res. 7, 387–413.
Wood, C.A., 1980b. Morphometric analysis of cinder cone degradation. J. Volcanol. Geotherm. Res. 8, 137–160.